Kidney360

Automated Image Analyses of Glomerular Hypertrophy in a Mouse Model of Diabetic Nephropathy

Mette V. Østergaard, Frederikke E. Sembach, Jacob L. Skytte, Urmas Roostalu, Thomas Secher, Agnete Overgaard, Lisbeth N. Fink, Niels Vrang, Jacob Jelsing, and Jacob Hecksher-Sørensen

Abstract

Background Glomerular hypertrophy is a hallmark of kidney injury in metabolically induced renal diseases such as obesity-associated glomerulopathies and diabetic nephropathy (DN).

Methods Using light sheet fluorescent microscopy (LSFM) and 3D image analysis, we tested algorithms for automated and unbiased quantification of total glomerular numbers and individual glomerular volume in the uninephrectomized (UNx) db/db mouse model of DN.

Results At 6 weeks after surgery, db/db and UNx db/db mice showed increased urine albumin-to-creatinine ratio (ACR) compared with db/+ control mice. Before euthanasia, glomeruli were labeled *in vivo* by injecting tomato lectin. Whole-kidney LSFM 3D image analysis revealed that mean glomerular volume was significantly increased in UNx db/db mice compared with db/+ mice. Moreover, analysis of individual glomerular volume showed a shift in volume distribution toward larger glomeruli and thereby demonstrated additive effects of diabetes and UNx on induction of glomerular hypertrophy. The automatized quantification showed no significant differences in glomerular numbers among db/+, db/db, and UNx db/db mice. These data correlated with glomerular numbers as quantified by subsequent stereologic quantification.

Conclusions Overall, LSFM coupled with automated 3D histomorphometric analysis was demonstrated to be advantageous for unbiased assessment of glomerular volume and numbers in mouse whole-kidney samples. Furthermore, we showed that injection of fluorescently labeled lectin and albumin can be used as markers of nephron segments in the mouse kidneys, thus enabling functional assessment of kidney physiology, pathology, and pharmacology in preclinical rodent models of kidney disease.

KIDNEY360 1: 469–479, 2020. doi: https://doi.org/10.34067/KID.0001272019

Introduction

Glomerular number and volume are key measurements in renal physiology and pathology. Although the total number of glomeruli is a fundamental parameter of kidney function, glomerular hypertrophy is a hallmark of kidney injury in metabolically induced renal diseases such as obesity-associated glomerulopathies and diabetic nephropathy (DN). Glomerular hypertrophy is caused by glomerular hypertension and hyperfiltration (1,2) and precedes the development of glomerulosclerosis and resulting renal impairment (3). In animal models of DN (4) and other kidney diseases (5,6), glomerular hypertrophy is an early marker of kidney disease and serves as a proxy for severity of kidney injury. Thus, assessment of glomerular volume is an important end point in basic and preclinical research.

The C57BLKS db/db mouse is a widely used model of DN in the setting of type 2 diabetes but develops only mild DN with moderate albuminuria and mesangial matrix expansion. Unilateral nephrectomy (UNx) accelerates DN in C57BLKS db/db mice, resulting in increased albuminuria and mesangial expansion, as well as tubular atrophy and dilation (7,8). Experimental stressors such as UNx and hypertension also aggravates glomerular hypertrophy in mouse models of DN (9,10). Quantification of glomerular number and volume in the rodent kidney has traditionally been performed using sectioning and stereology, which is labor intensive and time consuming (11,4). Novel methods based on whole-organ imaging by light sheet fluorescence microscopy (LSFM) and three-dimensional (3D) image analyses offer unbiased and automated assessment of the glomerular number and volumes in the intact mouse kidney (12). Here, we established a method using LSFM-based 3D image analysis to characterize changes in glomerular number and volume in response to diabetes and UNx in the db/db mouse model of DN. We also explore the future use of LSFM and whole-organ 3D imaging for assessment of functional renal end points.

Materials and Methods

Animals Housing and Surgical Procedures

All animal experiments were conducted in accordance with internationally accepted principles for the care and use of laboratory animals. The study was

Gubra ApS, Hørsholm, Denmark

Correspondence: Dr. Mette V. Østergaard or Dr. Jacob Hecksher-Sørensen, Gubra ApS, Hørsholm Kongevej 11B, DK-2970 Hørsholm, Denmark. E-mail: mvo@gubra.dk or jhs@gubra.dk

approved by the Danish Committee for Animal Research and covered by an institutional license (permit number: 2013-15-2934-00843). Animals (JanVier, Le Genest-Saint-Isle, France) were acclimatized for at least 1 week before the start of the study and kept in a light-, temperature-, and humidity-controlled room (12-hour light/dark cycle, 22–24° C, and 50% relative humidity). The animals had free access to standard chow diet and tap water throughout the experiments.

UNx and sham surgery were performed in 18-week-old male C57BLKS/J db/db mice, and age-matched unoperated db/+ mice served as controls. For UNx surgery, mice were anesthetized by isoflurane inhalation and a small incision was made to the left of the spine to expose the kidney. The left ureter, kidney artery, and kidney vein were identified and ligated with suture, after which the left kidney was removed. For sham surgery, the left kidney was exposed and gently manipulated, but without ligation or removal of the kidney. During postoperative recovery, mice received 5 mg/kg enrofloxacin and 5 mg/kg carprofen administered subcutaneously for 2 days. UNx and sham-operated db/db mice and unoperated db/+ controls were euthanized 6 weeks after surgery (at an age of 24 weeks) for whole-organ analyses by LSFM and 3D imaging.

For qualitative, functional 3D imaging, naive wild-type male C57BL/6J mice were euthanized at 10 weeks of age.

Blood and Urine Analyses

Blood glucose was measured by collecting blood from the tail vein of nonfasted mice into heparinized glass capillary tubes and immediately suspending in glucose/lactate system solution buffer (EKF Diagnostics, Barleben, Germany). Blood glucose was measured using a BIOSEN c-Line glucose meter (EKF Diagnostics) according to the manufacturer's instructions. Spot urine samples were collected directly from the penis to determine the urine albumin-to-creatinine ratio (ACR). Urine creatinine was measured using the CREP2 kit (Roche Diagnostics, Mannheim, Germany) on a Cobas C-501 autoanalyzer. Urine albumin was measured using a Mouse Albumin ELISA Kit (Bethyl Laboratories, Montgomery, TX).

Terminal *In Vivo* Injection of Fluorescently Labeled Molecules and Sample Preparation

Mice were anesthetized with subcutaneous injection of fentanyl/fluanisone (fentanyl 788 μg/kg, fluanisone 25 mg/kg) and midazolam (12.5 mg/kg). Following confirmation of anesthesia, db/+, db/db, and UNx db/db mice were slowly (over 20–30 seconds) injected in the tail vein with 0.1 ml of 1 mg/ml of DyLight-594–conjugated *Lycopersicon esculentum* (tomato) lectin (LEL; Vector Laboratories, Burlingame, CA), which binds to endothelial cells and labels blood vessels including the glomerular capillaries (13). C57BL/6J mice were injected with DyLight-649–conjugated LEL and Alexa Fluor 555–conjugated BSA (Thermo Fisher Scientific, Roskilde, Denmark). After 5 minutes, the mice were transcardially perfused with heparinized (15,000 IU/L) PBS for 2–3 minutes and then with 10% neutral-buffered formalin for 5 minutes, both at perfusion rates of 20 ml/min. After perfusion, the right kidney was dissected and the capsule was removed and postfixed with 10% neutral-buffered formalin overnight at room temperature (RT). Kidneys were dehydrated at RT in a methanol/water series (20%, 40%, 60%, 80%, 100% for 1 hour each) and transferred to fresh 100% methanol for an overnight incubation at RT. The following day, samples were incubated in 66% dichloromethane/33% methanol for 3 hours at RT and subsequently washed twice for 15 minutes in 100% dichloromethane before clearing overnight in dibenzyl ether. The kidneys were weighed before and after clearing, and the weight reduction in response to clearing was 39% in the db/+, 40% in the db/db, and 43% weight reduction in the UNx db/db.

LSFM and 3D Imaging

Kidneys were imaged on a LaVision Ultramicroscope II (Miltenyi Biotec, Bergisch Gladbach, Germany) setup equipped with MV PLAPO 2XC objective (Olympus, Tokyo, Japan), Zyla 4.2P-CL10 sCMOS camera (Andor Technology, Belfast, United Kingdom), and a SuperK EXTREME supercontinuum white-light laser EXR-15 (NKT Photonics, Birkerød, Denmark). For scanning, a customized silicone sample holder was made for this study. Silicone was prepared from the Sylgard 184 Silicone Elastomer Kit (Dow Silicones, Wiesbaden, Germany) according to manufacturer's specifications and poured over the LaVision sample holder, after removing the sample placement insert. The silicone was hardened for 12 hours at 50°C, generating a transparent flat surface on top of which samples could be mounted. The dibenzyl ether–cleared kidney was placed on the Sylgard silicone surface using a droplet of transparent neutral silicone gel (Dana Lim, Køge, Demark). The silicone/tissue interface is prone to light scatter, so it is important minimize the amount of silicone used for mounting for optimal image quality. Single-channel lectin imaging was carried out at 0.8× magnification (1.6× total magnification) with an exposure time of 161 ms in a z-stack at 10-μm intervals, using 595±20 nm excitation and 650±50 nm emission wavelengths. Contrast-based merging of horizontal focusing was used. Kidneys were imaged in two tiles with 20% overlap and merged into a single 3D image stack before image analysis. The size of a voxel in this study was 3.77×3.77×10 μm, giving a volume of 142.54 μm^3 (Supplemental Figure 1). In the healthy db/+ control mice, the median size of a glomerulus is 91,400 μm^3, corresponding roughly to 650 voxels, whereas the median size in the UNx db/db mice is 1100 voxels per glomerulus.

For simultaneous imaging of fluorescent LEL and BSA, 560±40 nm excitation and 620±60 nm emission wavelengths were used for Alexa Fluor 555–conjugated BSA, and 630±30 nm excitation and 680±30 nm emission wavelengths were used for DyLight-649–conjugated LEL. A selected area was imaged at 6.4× and 10× total magnification to reveal the fine morphology of proximal tubules.

Quantitative and Qualitative 3D Image Analyses

Using the lectin channel as reference, the entire kidney as well as the perfused glomeruli were segmented from the full image volume. As a preprocessing step, the lectin channel image was median filtered. To segment out the kidney from the background, Otsu thresholding was applied, and subsequent

morphologic closing was used to fill out potential holes in the segmentation mask.

For the glomerular segmentation, bright round objects were initially detected by applying a blob detector in a slice-by-slice fashion. Blobs were filtered according to size and intensity, and the blob centroids were saved. Hereafter, a gradient image for the lectin channel was calculated and passed, alongside the blob centroids, to a seeded 3D watershed algorithm. For each label in the resulting watershed segmentation image, the volume was calculated and regions that had an equivalent spherical diameter >40 μm were defined as a glomerulus and kept in the final segmentation mask. To incorporate spatial information in the glomerular measures, a Euclidean distance transform was applied to the kidney segmentation mask, which provided an estimated distance to kidney surface at each voxel location. Combining this distance map and the segmentation mask of the perfused glomeruli allowed for spatially resolved glomeruli measures.

To segment out the cortical and medullary compartments of the kidney, the spatial information of the individual glomeruli was further utilized. Using the fact that most glomeruli are located in the cortex area, the 95th percentile of the distance-to-surface distribution for all individual glomeruli can be used as a threshold value in the distance map to define the cortex. Everything below the threshold (closer to the kidney surface) was then considered to be cortex, and everything above the threshold (farther from the kidney surface) was considered medulla. Additionally, the glomeruli were removed from the cortex and medulla segmentation masks and a small margin was added between all three segmentation masks by morphologic erosion, resulting in the segmentation of three distinct renal compartments: glomeruli, cortex, and medulla.

The entire quantification pipeline is summarized in Supplemental Figure 2, and everything was implemented and automated using Python (https://www.python.org/). A full example script is provided at https://github.com/Gubra-Aps.

Quantification of Glomerular Number by Stereology and 3D-2D Correlation

To verify the results from LSFM and 3D image analysis, the number of glomeruli was estimated in UNx db/db mice using unbiased stereology. Briefly, after LSFM, the cleared kidneys were rehydrated at RT in 100% methanol followed by 1 hour incubation steps in an ethanol/water series of 99%, 96%, and 70%. Kidneys were cut transversely into 2-mm slabs in a systematic, uniform random sampling fashion using a razor blade fractionator and a random starting position. The resulting four to five slabs per kidney were dehydrated and infiltrated with paraffin in a tissue processor (VIP5; Sakura, Brøndby, Denmark) and then embedded with the cut surface down. Sections of 3 μm were cut on a microtome and collected on microscope slides in pairs with a disector distance of 12 μm. Periodic acid–Schiff staining was performed using standard procedures. Briefly, kidney sections were deparaffinized and oxidized in 0.5% periodic acid (Sigma-Aldrich, Søborg, Denmark). Next, sections were incubated with Schiff's reagent (Sigma-Aldrich) and counterstained with Mayer hematoxylin (Dako, Glostrup, Denmark). Sections were dehydrated and mounted with Pertex (Histolab, Gothenburg, Sweden). The total number of glomeruli was estimated by the physical disector using the principles developed by Gundersen and Jensen (14) on pairs of sections. Periodic acid–Schiff–stained slides were scanned under a 20× objective in an Aperio Scanscope AT slide scanner and imported into the stereology module of the Visiopharm Integrator Software (Visiopharm, Hørsholm, Denmark). The disector counting frame and sampling frequency was adjusted, allowing for an appropriate sampling density, and was used to count all glomeruli appearing in the reference section and not in the lookup section.

The image correlation between 2D and 3D sections was done manually using the oblique slicer feature in Imaris.

Histochemical and Immunohistochemical Stains

To test if processing of kidneys for LSFM was compatible with histochemical and immunohistochemical (IHC) staining protocols, hematoxylin and eosin (H&E), Picro-Sirius Red (PSR), and IHC stains were performed using standard procedures. Briefly, for hematoxylin and eosin staining, kidney sections were incubated in Mayer hematoxylin, washed in tap water, and stained in Eosin Y solution (Sigma-Aldrich) before dehydration and mounting with Pertex. Sections were incubated in Weigert iron hematoxylin (Sigma-Aldrich) and stained in PSR before dehydration and mounting with Pertex for PSR staining.

For IHC stains, antigen retrieval was performed in TRIS-EDTA-Glucose, pH 9.0, for 30 minutes at 98°C and cooled for 10 minutes. Primary antibodies were diluted in blocking buffer (0.5% Tris-buffered saline/Tween 20, 1% BSA, and 5% swine serum) and incubated overnight at 4°C. After incubation with horseradish peroxidase–conjugated secondary antibodies, the signal was developed using Liquid DAB+ Substrate Chromogen System (Dako). The primary antibodies and dilutions used were rabbit anti-podocin (1:100; catalog number P0372; Sigma-Aldrich), goat anti-collagen IV (1:100; catalog number 1340-01; Southern Biotech), and rabbit anti-Wilms tumor 1 (1:600; catalog number ab89901; Abcam).

Statistical Analyses

Results are presented as mean±SEM unless otherwise specified. For comparison of data between groups, one-way analysis with Tukey multiple comparisons test was used to test differences between groups. Urine ACR values were $\log_{10}$-transformed before group comparisons. A P-value <0.05 was considered statistically significant.

Results

Accelerators of Kidney Disease Induce Renal and Glomerular Hypertrophy in db/db Mice

In vivo measurements confirmed obesity and hyperglycemia in both db/db and UNx db/db mice compared with db/+ control mice (both $P<0.001$) (Table 1). Urine ACR was significantly increased in db/db mice with or without UNx compared to db/+ mice (both $P<0.05$), but albuminuria was not exacerbated in UNx db/db mice compared with db/db mice. The kidney weight tended to be increased in db/db compared with db/+ mice, without reaching statistical

Table 1. ***In vivo*** **measurements 6 wk after unilateral nephrectomy or sham surgery in db/db mice and in age-matched db/+ mice**

Measurement	db/+ (n=2)	db/db (n=7)	UNx db/db (n=9)
Body weight (g)	30.1±1.1	58.4±2.3[a]	56.1±1.5[a]
Blood glucose (mM)	6.56±1.93	29.7±2.1[a]	26.4±1.3[a]
Urine ACR (μg/mg)	43.7±7.5	698±301[b]	561±244[b]
Kidney weight (mg)	306±7	350±14	453±20[c,d]

Values are expressed as mean±SEM. UNx, unilateral nephrectomy; ACR, albumin-to-creatinine ratio.
[a]P<0.001 versus db/+.
[b]P<0.05 versus db/+.
[c]P<0.01 versus db/+.
[d]P<0.01 versus db/db.

significance, whereas UNx db/db mice displayed increased kidney weight compared with db/+ and db/db mice (both P<0.01). To summarize, *in vivo* measurements indicated that UNx did not worsen obesity, hyperglycemia, or albuminuria in db/db mice, but did induce renal hypertrophy.

To further investigate the effects of diabetes and UNx on the morphology of kidney and glomeruli, we used LSFM and 3D whole-kidney imaging to reconstruct and visualize the complete population of glomeruli in kidneys from db/+, db/db, and UNx db/db mice after intravenous (i.v.) injection of fluorescently labeled LEL (Figure 1, A–C). A volume-based color code was used to visualize the volume of each individual glomerulus demonstrating a shift toward larger glomerular volumes in db/db and UNx db/db mice compared with db/+ mice (Figure 1, A′–C′).

Based on virtual 3D reconstruction and image analyses, db/db mice displayed renal hypertrophy as compared with normoglycemic db/+ mice (192.6±6.3 versus 143.0±14.6 mm^3, P<0.05), whereas UNx tended to further augment renal hypertrophy in db/db mice (230.8±12.2 mm^3, P=0.056 versus db/db) (Figure 1D). The total number of glomeruli per kidney was 14,126±950 in db/+ mice versus 15,908±1240 in db/db mice and 15,332±269 in UNx db/db mice and thus did not significantly differ between groups (Figure 1E). To verify the glomerular number determined by automatized 3D image analysis, we assessed glomerular number by stereology in a subset of kidneys after completion of LSFM. Stereologic analysis yielded similar estimates of whole-kidney glomerular numbers (Figure 1F).

Quantification of glomerular volume based on volumetric segmentation demonstrated that mean glomerular volume was not significantly different in db/db mice versus db/+ mice (129,000±15,700 versus 99,773±9060 μm^3) (Figure 1G). However, glomerular volume was significantly increased in UNx db/db mice (163,000±10,100 μm^3) compared with both db/+ (P<0.001) and db/db mice (P<0.05), indicating marked glomerular hypertrophy in UNx db/db mice (Figure 1G). Although diabetes alone did not significantly affect mean glomerular volume in db/db mice compared with normoglycemic db/+ mice, a distribution plot of the number of glomeruli as a function of glomerular volume demonstrated a shift in volume frequency distribution from db/+ mice to db/db mice, and further from db/db mice to UNx db/db mice (Figure 1H). Thus, application of 3D image analysis and frequency distribution plots demonstrates additive effects of diabetes and UNx on induction of glomerular hypertrophy in db/db mice.

Cortical Localization of Glomeruli Affects Their Sensitivity to Accelerators of Kidney Disease

To investigate glomerular hypertrophy in further detail, we investigated the effect of diabetes and UNx on glomerular volume with respect to their spatial location within the renal cortex. Using volume-based color codes to visualize the volume of each individual glomerulus in db/+ mice, glomeruli located in the superficial cortex appear smaller (blue/green color code) compared with juxtamedullary glomeruli within the same mouse (yellow/red color code) (Figure 2A). This observation was evident for all three groups. The precise spatial coordinates of each individual glomerulus allowed for a spatial distribution analysis based on the shortest distance from the center of a glomerulus to the surface of the kidney (Figure 2, B and C). In all groups, distance-to-surface frequency plot (Figure 2D) revealed that most glomeruli are located within approximately 400 μm from the surface of the processed kidney and that very few glomeruli are localized >1200 μm from the kidney surface (Figure 2D). Thus, the thickness of the renal cortex, defined as the region in which glomeruli are localized within the kidney, did not significantly change under conditions of kidney hypertrophy. In contrast, spatial volume distribution revealed significant differences in glomerular volume throughout the cortex among study groups (Figure 2E). Accordingly, glomerular hypertrophy occurred throughout the entire renal cortex in db/db mice with or without UNx, as compared with db/+ mice (P<0.05). Furthermore, in UNx db/db mice, glomerular hypertrophy was exacerbated compared with db/db mice (P<0.05), but only in the superficial cortex (<600 μm from the kidney surface).

LSFM is Compatible with Histologic and IHC Staining Procedures

A limitation of whole-organ and 3D image analyses is the number of end points that can be analyzed simultaneously due to the limited number of fluorescence channels available. We therefore assessed the applicability of performing subsequent conventional histologic analyses on tissue sections from LSFM-imaged kidneys. Representative images of

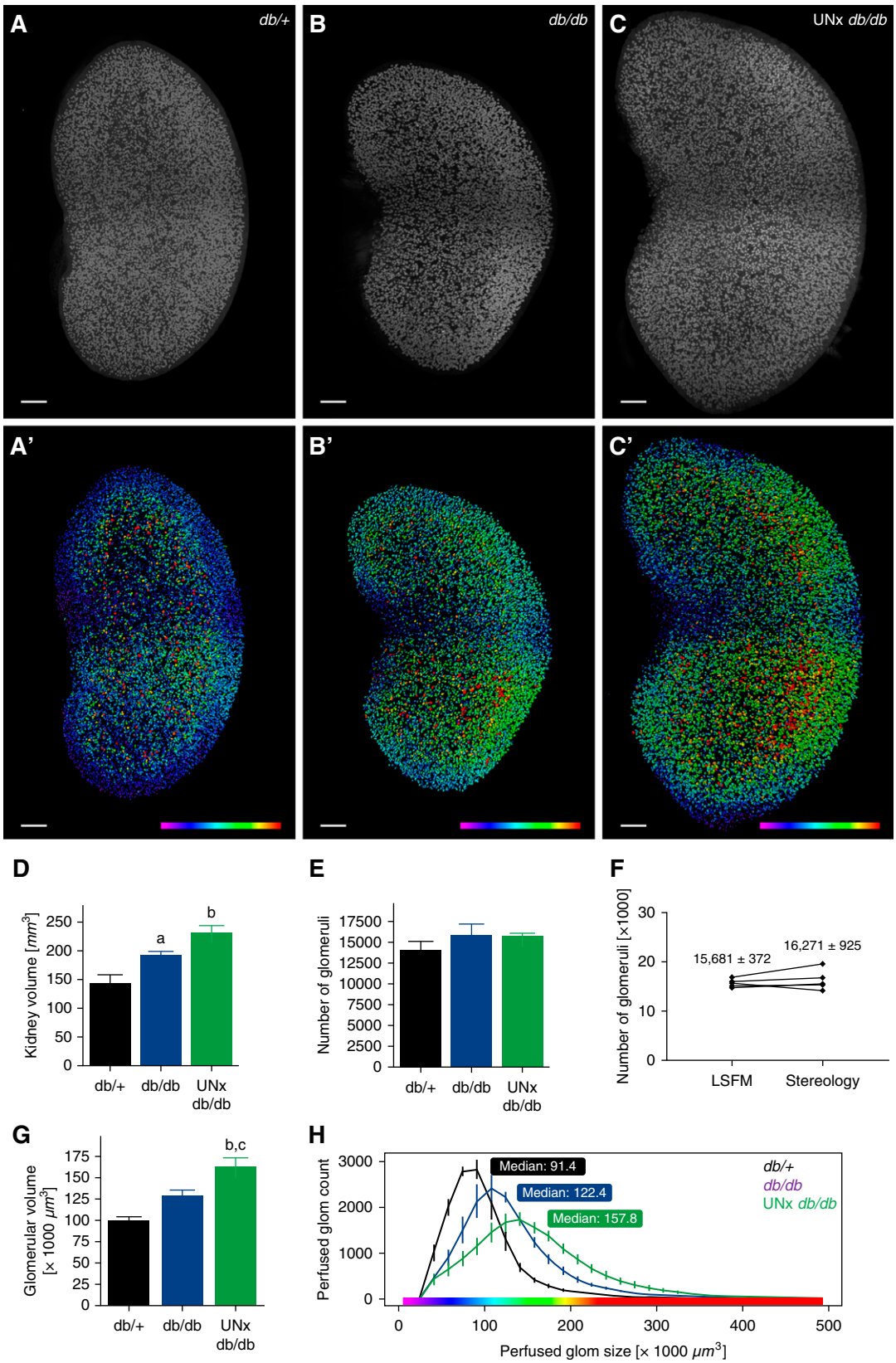

Figure 1. | Quantification of glomeruli number and glomerular volume using light sheet microscopy (LSFM) and three-dimensional (3D) image analyses. (A–C) 3D reconstruction of representative kidneys from db/+, db/db, and uninephrectomized (UNx) db/db mice, respectively. (A′–C′) Volume rendered and color-coded images of the same kidneys. Scale bar, 500 μm. (D) Absolute kidney volume (mm^3). (E) Number of glomeruli per kidney as determined by 3D image analyses and (F) comparison of glomeruli count as assessed by LSFM and stereology from the

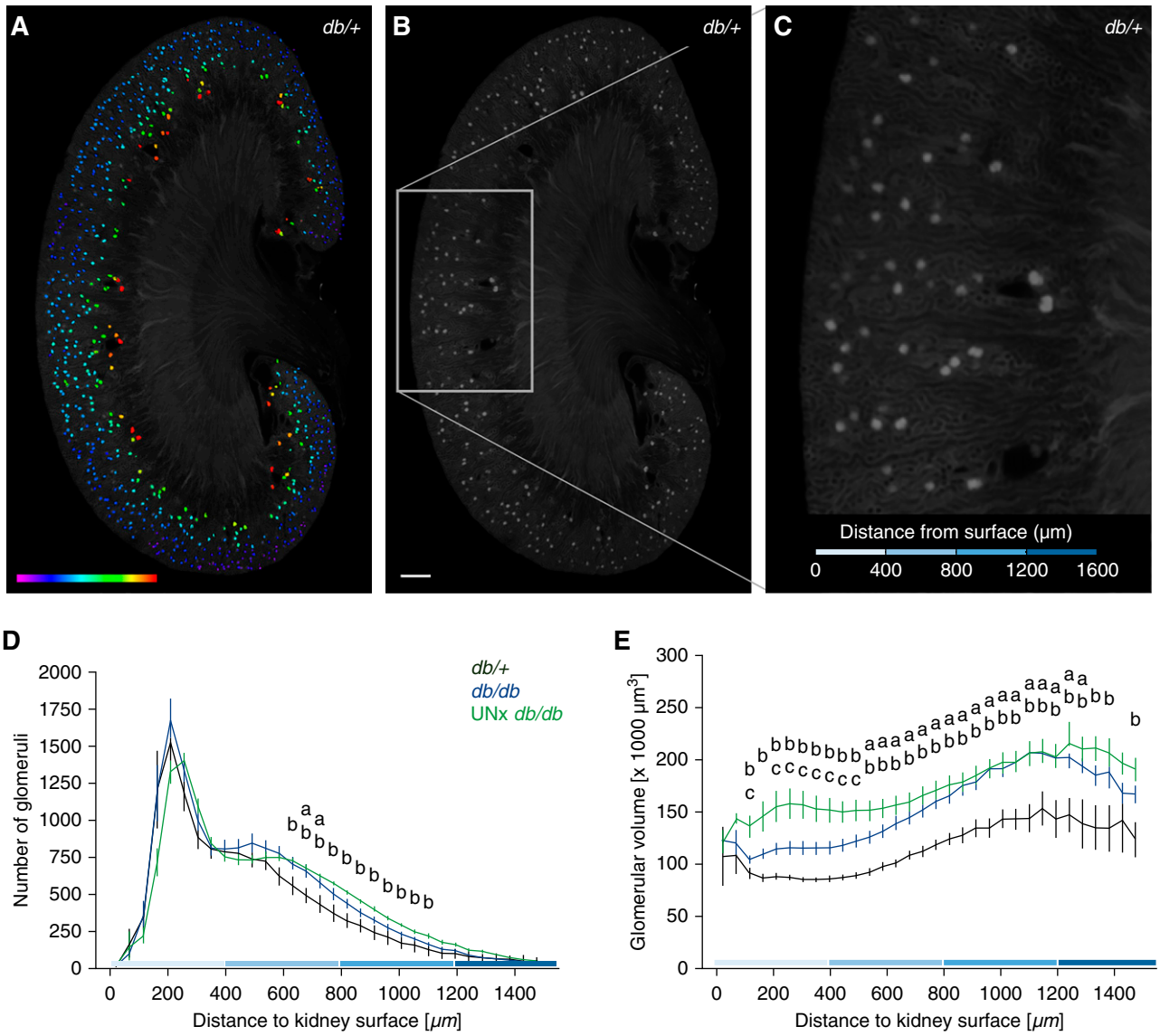

Figure 2. | Characterization of hypertrophy in superficial and juxtamedullary glomeruli. (A) Sagittal section (100 μm thick) through a representative db/+ mouse kidney and color coding of glomeruli according to glomerular volume. Volume color coding rages from 50 (blue) to 300 $\times$1000 μm^3 (red). (B) The lectin signal from the same kidney at low magnification. Scale bar, 500 μm. (C) High magnification of the highlighted area shown in B. The scale bar shows the distance from the surface of the kidney in 500 μm intervals. (D) Frequency distribution plot of glomerular distance from the kidney surface, demonstrating highest glomerular density in outer cortex and decreasing density toward the juxtamedullary zone. (E) Glomerular volumes quantified as a function of the distance to the kidney surface, demonstrating hypertrophy in diabetic db/db and UNx db/db mice independently of glomerular localization. UNx in db/db mice further exacerbates glomerular hypertrophy in the outer cortex, but not in juxtamedullary glomeruli. Data are mean±SEM. Superscript letters indicate statistically significant differences between groups: [a]$P<0.05$, db/db versus db/+; [b]$P<0.05$, UNx db/db versus db/+; [c]$P<0.05$, UNx db/db versus db/db.

LSFM-processed and subsequently paraffin-embedded kidney sections demonstrate that LSFM is compatible with subsequent histologic staining and analyses (Figure 3, A and B). Furthermore, IHC testing of antibodies for detection of fibrosis such as collagen IV (Figure 3C) as well as membranous and nuclear podocyte markers, including podocin and Wilms' tumor 1 (Figure 3, D and E) were all applicable in LSFM-processed, paraffin-embedded db/+ mouse kidneys. Thus, LSFM and 3D imaging enable automated whole-kidney morphologic analyses with the possibility to perform

same UNx db/db mice. (G) Glomerular volume (μm^3). (H) Frequency distribution plot of glomerular volumes from the three groups. Volume color coding (in (A′–C′)) ranges from approximately 30 (blue) to 300 $\times$1000 mm^3 (red). (D–H) Data are mean±SEM. Superscript letters indicate statistically significant differences between groups: [a]$P<0.05$, db/db versus db/+; [b]$P<0.05$, UNx db/db versus db/+; [c]$P<0.05$, UNx db/db versus db/db.

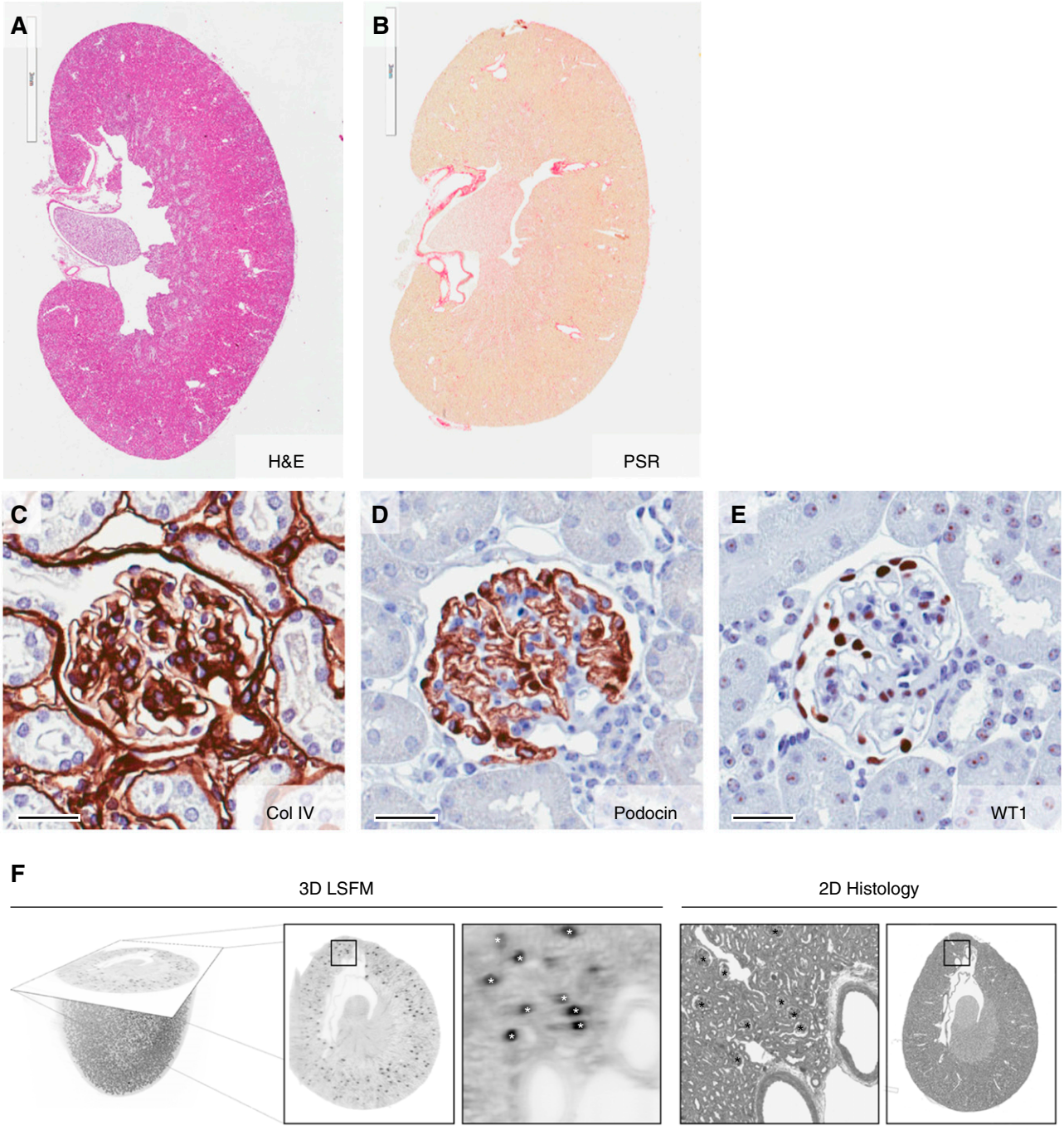

Figure 3. | **Histology and immunohistochemistry in kidney tissue processed for LSFM.** Sagittal sections from a representative kidney from a db/+ mouse initially processed for LSFM and subsequently paraffin embedded and stained with (A) hematoxylin and eosin (H&E) or (B) Picro-Sirius Red (PSR) for histopathologic assessment, and by immunohistochemistry stains for detection and quantification of renal (C) collagen IV (Col IV), (D) podocin, and (E) Wilms tumor 1 (WT1). (F) A given 2D section can be mapped back into its original position in the 3D reconstructed kidney. Glomeruli that can be found in both the 3D reconstructed section and in the 2D paraffin section are marked with *. Scale bars in (C and D), 20 μm.

subsequent histopathologic analysis by conventional IHC. Finally, we demonstrate that it is possible to map a given 2D section of a mouse kidney back to the corresponding position in the 3D reconstructed kidney (Figure 3F) and even to recover individual glomeruli. Thus, 3D imaging by LSFM supports combination of 3D and 2D histologic end points in the same kidney sample.

Qualitative and Quantitative Assessment of Renal Albumin Handling by 3D Imaging

Fluorescently labeled lectin and albumin was coinjected i.v. in healthy C57BL/6J mice. After 5 minutes, mice were euthanized, and kidneys were processed for LSFM imaging (Figure 4A). As shown previously, lectin marks the renal vasculature including the capillaries of the glomerulus

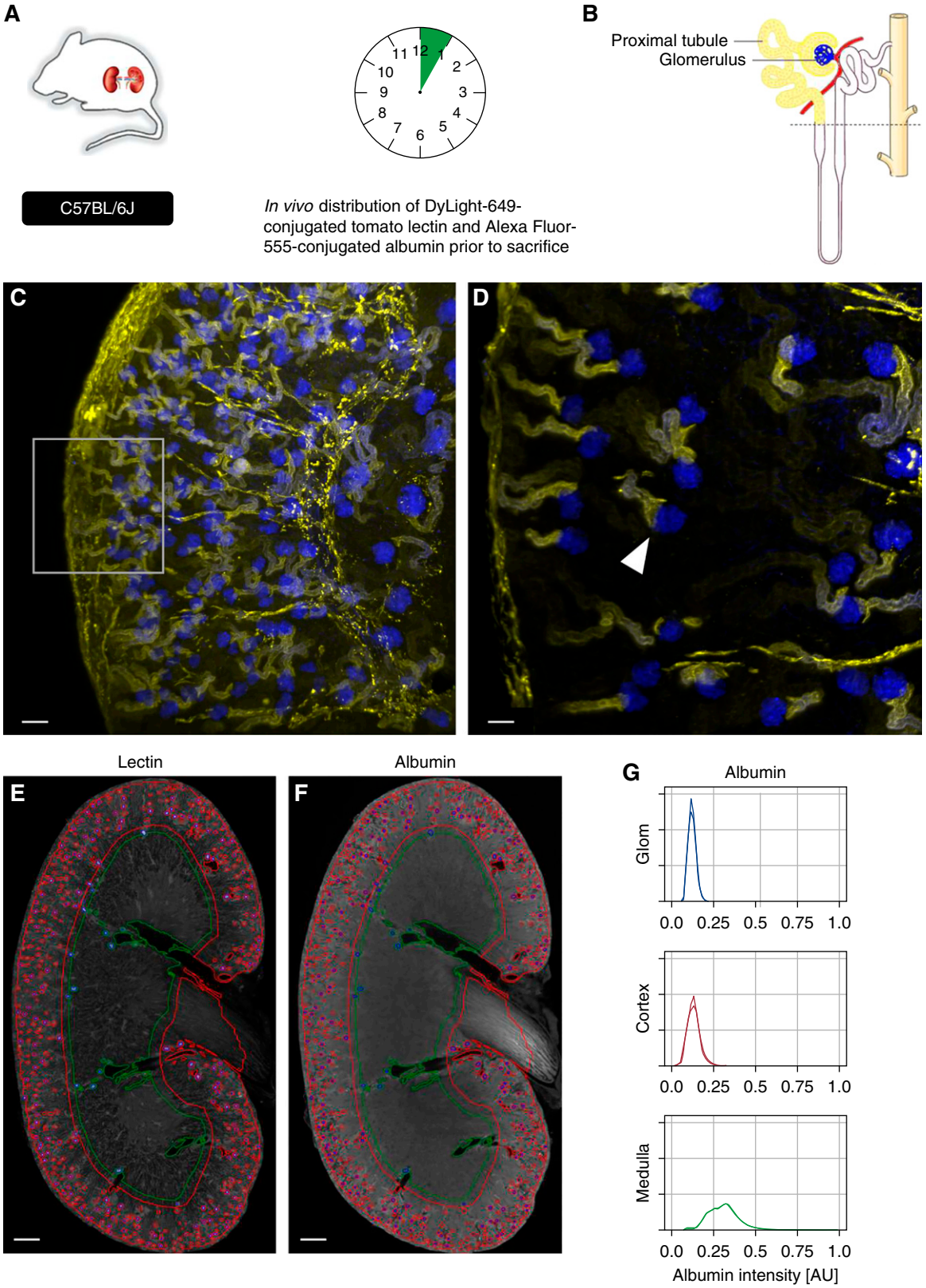

Figure 4. | **Visualization of the glomerulotubular junction by LSFM.** (A) Male C57BL/6 mice were injected with DyLight-649–conjugated tomato lectin and Alexa Fluor 555–conjugated albumin. After 5 minutes, right kidneys were sampled and processed for LSFM and 3D image reconstruction. (B) Schematic representation of labeling of the glomerulus and proximal tubule by lectin and albumin. Under normal physiologic conditions, lectin is bound with high density to the capillary endothelium of the glomerulus (in blue), while filtered albumin is absorbed in the proximal tubules of the nephron (in yellow). (C and D) LSFM imaging of a representative C57BL/6J mouse kidney showing lectin-

(Figure 4, B and C, in blue), whereas albumin to a certain extent is filtered across the glomerular filtration barrier and reabsorbed by the proximal tubular epithelial cells (Figure 4, B and D, in yellow). Furthermore, for initial quantification of renal albumin handling, we established new algorithms to segment the renal cortex and medulla in addition to glomeruli. Firstly, using the lectin channel, the renal cortex and medulla were segmented based on the presence and absence of glomeruli, respectively (Figure 4E). Secondly, the three segmented renal compartments were applied to the data collected in the albumin channel (Figure 4F), enabling the quantification of albumin intensity in glomeruli, cortex, and medulla, respectively (Figure 4G). Thus, our established protocol for *in vivo* labeling and LSFM 3D imaging of functional compartments of the mouse kidney allows for implementation of automated analyses of both renal structural and functional end points.

Discussion

Glomerular hypertrophy is considered a hallmark of kidney disease in patients who are obese and diabetic. In this study, we developed a method based on LSFM 3D imaging to quantify the number and volumes of glomeruli in a mouse model of DN and establish algorithms to describe the spatial distribution of the glomerular population in the intact mouse kidney. Although the number of glomeruli per kidney remains unchanged, diabetic db/db mice—irrespective of UNx—display glomerular hypertrophy compared with normoglycemic db/+ mice. Notably, diabetes-induced glomerular hypertrophy is aggravated by UNx in db/db mice. Specifically, UNx accelerates hypertrophy in superficial, but not juxtamedullary, glomeruli in diabetic mice. The combination of LSFM and 3D imaging thus shows great promise for assessing therapeutic effects on glomerular morphometry and can be combined with standard histologic analysis. The use of multiple fluorescently labeled tracers may also allow for analyses of kidney function by assessing nephron albumin handling in the glomeruli and proximal tubules of the mouse kidney.

UNx is a well established experimental accelerator of kidney injury in animal models of renal disease, especially in models of DN. Here, the db/db mouse model with or without UNx was used as a model to characterize quantitative changes in glomerular number and volume by LSFM and 3D imaging. Although db/db mice (with or without UNx) displayed increases in urine ACR as compared with healthy db/+ mice, the short postsurgery period (6 weeks) may explain why albuminuria was not augmented by UNx in db/db mice, as shown previously at 18 weeks after UNx (7).

The estimation of absolute glomerular numbers in a kidney is of interest because of the association between low glomerular numbers (and hence low nephron numbers) and development of kidney disease (15,16). However, in mouse models with features of early DN and mild kidney injury such as the UNx db/db mouse model, the number of glomeruli is not expected to be affected (17), which was also demonstrated in this study. Interestingly, despite the lack of changes in glomerular numbers among all groups and lack of an increase in albuminuria between db/db and UNx db/db specifically, we demonstrated marked alterations in renal and glomerular hypertrophy in diabetic db/db compared with healthy db/+ mice and, furthermore, that glomerular hypertrophy is augmented by UNx in db/db mice. Thus, our data demonstrate the applicability of LSFM and 3D imaging as a sensitive method for quantification of structural and morphometric end points at the whole-organ level in mouse models of renal disease.

The spatial volume distribution that demonstrates increasing volume from the superficial to the juxtamedullary glomeruli is in alignment with findings in human subjects with and without kidney disease (18,19). Similarly, the advanced glomerular hypertrophy in the superficial glomeruli as compared with the juxtamedullary glomeruli of UNx mice corresponds nicely with patient data, where glomerulosclerosis in seen to affect a larger percentage of superficial versus juxtamedullary glomeruli (18,19). To our knowledge, these are the first data to decipher the glomerular hypertrophy in response to experimental accelerators of kidney injury as a function of their localization in the renal cortex.

Stereology is considered the gold standard for unbiased assessment of quantitative morphologic changes such as glomerular hypertrophy. However, besides being very time consuming, stereologic assessment of individual glomeruli volume and total glomerular numbers represents estimates with only group means approaching the true value. The application of LSFM and 3D imaging in combination with automated quantitative image analysis enables fast assessment of whole-kidney absolute glomerular numbers. To validate the results from the automatized 3D image analyses, mean glomerular numbers were compared to stereologic estimates based on the physical dissector principle (20) on the same kidney. The analyses revealed highly similar average glomerular numbers, confirming concordance of the automatized LSFM and 3D imaging-based technology with current stereology-based estimates (21,22). Finally, several histochemical and IHC stains were performed on the mouse kidneys that were initially cleared for and subjected to LSFM, confirming that whole-organ imaging is compatible with classic 2D histopathologic assessment for several end point analyses.

In previous 3D imaging studies, staining of glomeruli has been achieved using *in vivo* labeling of the vasculature and glomerular capillaries using labeled anti-CD31 antibodies (23). In this study, an endothelial cell-binding lectin, LEL, was injected i.v. 5 minutes before euthanasia to enable visualization of the mouse vasculature including the glomerular capillaries. Both methods eliminate the need for

labeled glomeruli and filtered albumin absorbed in the proximal tubule in yellow at low and high magnification, respectively. Arrowhead represents the glomerulotubular junction. Scale bars, 100 μm (C) and 50 μm (D). (E and F) Segmentation of glomeruli (blue), cortex (red), and medulla (green) in a representative C57BL/6J mouse kidney. Scale bar, 500 μm. The segmentation is based on the localization of glomeruli as determined using (E) the lectin channel and subsequently applied to (F) the albumin channel. (G) Histograms of albumin intensities as a measure of albumin content in the three renal compartments in a representative C57BL/6J mouse kidney.

antibody incubation and reduce experimental timelines considerably (24). However, it should be noted that *in vivo* labeling of glomeruli may be incomplete in animal models with more severe kidney disease such as models of late stage DN and CKD. In these animal models, global glomerulosclerosis in a subpopulation of glomeruli may affect the perfusion efficiency or the labeling of glomerular endothelial cells. In such cases, only perfusable glomeruli will be identified by the algorithm and the estimated loss of labeled glomeruli may be used as a proxy for loss of functional nephrons. Furthermore, the tracing of renal structures (*e.g.*, individual glomerulus) between 2D histologic sections and the 3D reconstructed kidney allows for the combination of traditional histopathologic end points and the structural and functional end points as measured by 3D imaging. For example, traditional glomerulosclerosis scores could be correlated with 3D imaging quantification of glomerular perfusion and albumin filtration, allowing for the combination and correlation of 2D and 3D end points.

Although two-photon imaging has recently been applied to study absorption of albumin in the proximal tubules (25), use of LSFM for functional imaging of the mouse kidney has been limited. As a proof of concept, we established a protocol for *in vivo* injection of fluorescently labeled lectin and albumin in wild-type C57BL/6J mice followed by perfusion fixation and clearing of kidneys before LSFM. Furthermore, we established algorithms for initial quantification of albumin intensity in the three renal structural compartments of the glomeruli, the cortex, and the medulla. Thus, we demonstrate that i.v. injection of multiple fluorescently labeled tracers in the live animal holds the potential to investigate functional readouts by LSFM and subsequent image analysis including glomerular, cortical, and medullary albumin intensity in addition to structural end points such as glomerular volume and numbers. The algorithms for the quantification of albumin filtration and absorption across the entire population of nephrons in a mouse kidney are currently being further developed to fully exploit the potential of LSFM and 3D image analysis in kidney physiology, pathology, and pharmacology assessments in preclinical rodent models of kidney disease.

Acknowledgments

The authors would like to thank Katja Birch Hansen, Martin Mikkelsen, Malene Anja Christiansen, Lotte Ankjær Frederiksen, Lotte Handgaard Jørgensen, and Mette Musfelth Nebbelunde for excellent technical assistance.

Author Contributions

L. Fink, J. Hecksher-Sørensen, J. Jelsing, U. Roostalu, N. Vrang, and M. Østergaard conceptualized the study; J. Hecksher-Sørensen and U. Roostalu were responsible for methodology; J. Hecksher-Sørensen, U. Roostalu, J. Skytte, and M. Østergaard wrote the original draft and were responsible for visualization; J. Jelsing reviewed and edited the manuscript; A. Overgaard, T. Secher, and F. Sembach were responsible for investigation; U. Roostalu and J. Skytte were responsible for data curation; T. Secher, F. Sembach, and T. Secher were responsible for formal analysis; and all authors approved the final version of the manuscript to be published.

Disclosures

All authors are current employees of Gubra ApS. L. Fink reports other from Novo Nordisk A/S outside the submitted work. J. Jelsing and N. Vrang are owners of Gubra. F. Sembach reports grants from Innovation Foundation outside the submitted work.

Funding

None.

Supplemental Material

This article contains supplemental material online at http://kidney360.asnjournals.org/lookup/suppl/doi:10.34067/KID.0001272019/-/DCSupplemental.

Supplemental Figure 1. Illustration of the resolution achieved with LSFM.

Supplemental Figure 2. Flow chart of the entire quantification pipeline.

References

1. D'Agati VD, Chagnac A, de Vries APJ, Levi M, Porrini E, Herman-Edelstein M, Praga M: Obesity-related glomerulopathy: Clinical and pathologic characteristics and pathogenesis. *Nat Rev Nephrol* 12: 453–471, 2016
2. Tobar A, Ori Y, Benchetrit S, Milo G, Herman-Edelstein M, Zingerman B, Lev N, Gafter U, Chagnac A: Proximal tubular hypertrophy and enlarged glomerular and proximal tubular urinary space in obese subjects with proteinuria. *PLoS One* 8: e75547, 2013
3. Reidy K, Kang HM, Hostetter T, Susztak K: Molecular mechanisms of diabetic kidney disease. *J Clin Invest* 124: 2333–2340, 2014
4. Guo M, Ricardo SD, Deane JA, Shi M, Cullen-McEwen L, Bertram JF: A stereological study of the renal glomerular vasculature in the db/db mouse model of diabetic nephropathy. *J Anat* 207: 813–821, 2005
5. Wei P, Lane PH, Lane JT, Padanilam BJ, Sansom SC: Glomerular structural and functional changes in a high-fat diet mouse model of early-stage Type 2 diabetes. *Diabetologia* 47: 1541–1549, 2004
6. Kren S, Hostetter TH: The course of the remnant kidney model in mice. *Kidney Int* 56: 333–337, 1999
7. Ninichuk V, Kulkarni O, Clauss S, AndersH-J: Tubular atrophy, interstitial fibrosis, and inflammation in type 2 diabetic db/db mice. An accelerated model of advanced diabetic nephropathy. *Eur J Med Res* 12: 351–355, 2007
8. Ninichuk V, Khandoga AG, Segerer S, Loetscher P, Schlapbach A, Revesz L, Feifel R, Khandoga A, Krombach F, Nelson PJ, Schlöndorff D, Anders HJ: The role of interstitial macrophages in nephropathy of type 2 diabetic db/db mice. *Am J Pathol* 170: 1267–1276, 2007
9. Mallipattu SK, Gallagher EJ, LeRoith D, Liu R, Mehrotra A, Horne SJ, Chuang PY, Yang VW, He JC: Diabetic nephropathy in a nonobese mouse model of Type 2 diabetes mellitus. *Am J Physiol Ren Physiol* 306: F1008–F1017, 2014
10. He X, Zhang T, Tolosa M, Goru SK, Chen X, Misra PS, Robinson LA, Yuen DA: A new, easily generated mouse model of diabetic kidney fibrosis. *Sci Rep* 9: 12549, 2019
11. Hughson MD, Hoy WE, Douglas-Denton RN, Zimanyi MA, Bertram JF: Towards a definition of glomerulomegaly: Clinical-pathological and methodological considerations. *Nephrol Dial Transplant* 26: 2202–2208, 2011
12. Klingberg A, Hasenberg A, Ludwig-Portugall I, Medyukhina A, Männ L, Brenzel A, Engel DR, Figge MT, Kurts C, Gunzer M: Fully automated evaluation of total glomerular number and capillary tuft size in nephritic kidneys using lightsheet microscopy. *J Am Soc Nephrol* 28: 452–459, 2017
13. Robertson RT, Levine ST, Haynes SM, Gutierrez P, Baratta JL, Tan Z, Longmuir KJ: Use of labeled tomato lectin for imaging vasculature structures. *Histochem Cell Biol* 143: 225–234, 2015

14. Hann BD, Baldelomar EJ, Charlton JR, Bennett KM: Measuring the intrarenal distribution of glomerular volumes from histological sections. *Am J Physiol Renal Physiol* 310: F1328–F1336, 2016
15. Hoy WE, Douglas-Denton RN, Hughson MD, Cass A, Johnson K, Bertram JF: A stereological study of glomerular number and volume: Preliminary findings in a multiracial study of kidneys at autopsy. *Kidney Int Suppl* 83: S31–S37, 2003
16. Sembach FE, Fink LN, Johansen T, Boland BB, Secher T, Thrane ST, Nielsen JC, Fosgerau K, Vrang N, Jelsing J, Pedersen TX, Østergaard MV: Impact of sex on diabetic nephropathy and the renal transcriptome in UNx db/db C57BLKS mice. *Physiol Rep* 7: e14333, 2019
17. Sasaki T, Tsuboi N, Okabayashi Y, Haruhara K, Kanzaki G, Koike K, Takahashi H, Ikegami M, Shimizu A, Yokoo T: Synergistic impact of diabetes and hypertension on the progression and distribution of glomerular histopathological lesions. *Am J Hypertens* 32: 900–908, 2019
18. Denic A, Ricaurte L, Lopez CL, Narasimhan R, Lerman LO, Lieske JC, Thompson RH, Kremers WK, Rule AD: Glomerular volume and glomerulosclerosis at different depths within the human kidney. *J Am Soc Nephrol* 30: 1471–1480, 2019
19. Sterio DC: The unbiased estimation of number and sizes of arbitrary particles using the disector. *J Microsc* 134: 127–136, 1984
20. Cullen-McEwen LA, Kett MM, Dowling J, Anderson WP, Bertram JF: Nephron number, renal function, and arterial pressure in aged GDNF heterozygous mice. *Hypertension* 41: 335–340, 2003
21. Chacon-Caldera J, Geraci S, Krämer P, Cullen-McEwen L, Bertram JF, Gretz N, Schad LR: Fast glomerular quantification of whole *ex vivo* mouse kidneys using Magnetic Resonance Imaging at 9.4 Tesla. *Z Med Phys* 26: 54–62, 2016
22. Puelles VG, Fleck D, Ortz L, Papadouri S, Strieder T, Böhner AMC, van der Wolde JW, Vogt M, Saritas T, Kuppe C, Fuss A, Menzel S, Klinkhammer BM, Müller-Newen G, Heymann F, Decker L, Braun F, Kretz O, Huber TB, Susaki EA, Ueda HR, Boor P, Floege J, Kramann R, Kurts C, Bertram JF, Spehr M, Nikolic-Paterson DJ, Moeller MJ: Novel 3D analysis using optical tissue clearing documents the evolution of murine rapidly progressive glomerulonephritis. *Kidney Int* 96: 505–516, 2019
23. Renier N, Wu Z, Simon DJ, Yang J, Ariel P, Tessier-Lavigne M: iDISCO: A simple, rapid method to immunolabel large tissue samples for volume imaging. *Cell* 159: 896–910, 2014
24. Schuh CD, Polesel M, Platonova E, Haenni D, Gassama A, Tokonami N, Ghazi S, Bugarski M, Devuyst O, Ziegler U, Hall AM: Combined structural and functional imaging of the kidney reveals major axial differences in proximal tubule endocytosis. *J Am Soc Nephrol* 29: 2696–2712, 2018

Received: January 17, 2020 **Accepted:** April 24, 2020

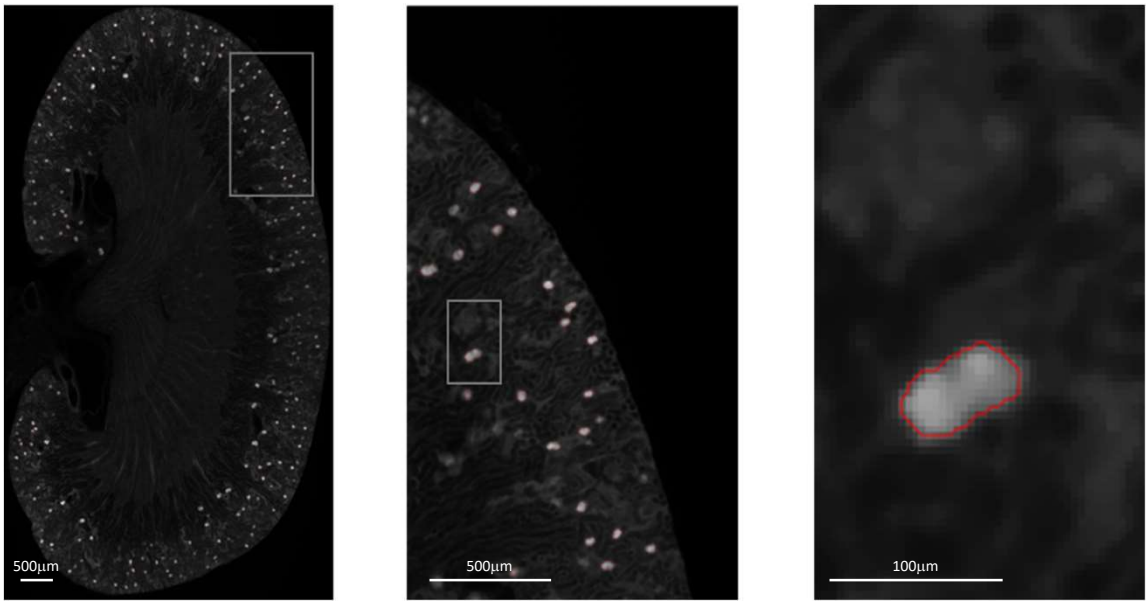

Supplementary figure 1: Illustration of the resolution achieved with LSFM. Zooming in on a glomeruli (squared box) it is possible to see the individual voxels. The size of a voxel in this study was 3.77 × 3.77 × 10 µm, giving a volume of 142.54 µm3 per voxel. In the control mice the median size of a glomerulus is 91400 µm3 which corresponds roughly to 650 voxels. The red line shows the glomeruli segmentation.

Supplementary figure 1

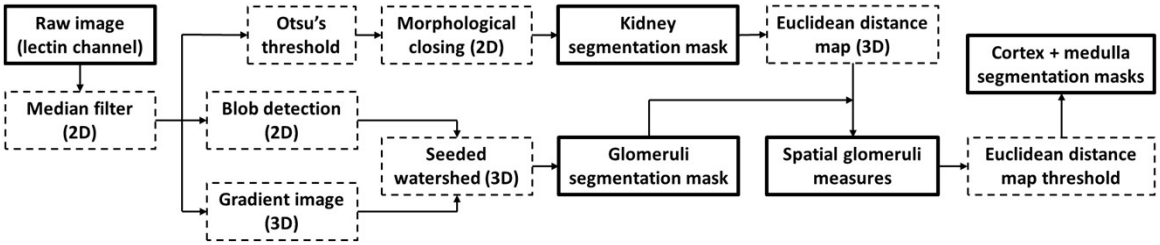

Supplementary figure 1: Flow chart of the entire quantification pipeline. Solid box outlines lines denotes data input/output, whereas dashed box outlines denotes operations.

Supplementary figure 2